

## Research Paper

# Evaluation of Measured Strain Responses to *in Situ* Vehicular Loading for Typical Asphalt Pavements

Chuan XIAO<sup>1), 2)</sup>

<sup>1)</sup> *Department of Transportation and Municipal Engineering  
Sichuan College of Architectural Technology  
Deyang, Sichuan 618000, China*

<sup>2)</sup> *Department of Civil and Environmental Engineering  
University of South Florida  
Tampa, FL 33620-4202, USA  
e-mail: chuanxiao@mail.usf.edu*

To characterize the dynamic behavior of typical asphalt pavements, which is induced by a complex loading system coupled with environmental effects, full-scale field tests were conducted on instrumented sections with embedded sensors. The impacts of vehicular loading factors and pavement temperature on strains at the bottom of asphalt layers were analyzed in the presence of *in situ* dynamic loading. According to orthogonal array tests, the impact levels of loading factors were quantified through analysis of variance. Furthermore, the temperature conversion factors of measured strain were explored using regression analysis. These results show that the measured strains present an asymmetry over time. The strain response goes up with increasing axle load and decreases with growing speed. Compared to the speed and the tire inflation pressure, the axle load plays a dominant role in strain responses. The estimated temperature conversion factor facilitates the strain conversion between non-standard temperature conditions and a required reference temperature.

**Key words:** asphalt pavement; measured strain response; vehicular loading; temperature; conversion factor.

## 1. INTRODUCTION

In the contemporary society, it is universally acknowledged that the mechanistic-empirical methodology used for pavement design has been playing an increasing role in helping highway infrastructure get access to superior value in terms of durability and performance [1, 2]. In light of the Mechanistic-Empirical Pavement Design Guide (MEPDG) [3], the accurate responses representing the dynamic properties of pavement structure are of great benefit to offer a suitable assessment of the present status and an accurate prediction of the further distresses.

As one example, the fatigue endurance limit regarding the cyclic traffic loading is dependent on the induced tensile strain at the bottom of the asphalt concrete (AC) layer based on some fatigue cracking failure criterion [4]. Therefore, the accuracy of strain responses is the paramount element in the success of pavement design system responsible for identifying the long-term pavement performance and avoiding unexpected fatigue distresses. The dynamic responses in flexible pavements are induced by a complex loading system [5]. It is due to measured results help to overcome the over-simplified or indeterminate elements of theoretical analysis that the full-scale measurement method has been playing an increasingly pivotal role in the assessment of dynamic behavior in pavements.

Researchers into the dynamic behavior of flexible pavements and optimization of the pavement design system have attempted to build full-scale instrumented test sections. Some of the well-known projects, particularly in the USA, including the AASHO Road Test carried out by the American Association of State Highway and Transportation Officials (AASHTO), National Center for Asphalt Technology (NCAT) Test Track, the Minnesota Road Research Project (Mn-Road), Virginia Smart Road, and Superpave *in situ* stress/strain investigation (SISSI) sponsored by the Pennsylvania Department of Transportation, have validated the feasibility and precision of full-scale field tests in pavement surface structure [6–10]. Accordingly, the overall objective of the study is to achieve a better understanding of structural dynamic response and performance of asphalt pavements under various loading and environmental conditions in China, so as to extend pavement service life and reduce maintenance costs.

## 2. STATE OF THE ART

The use of embedded sensors to monitor and measure *in situ* pavement response and performance has been developed markedly in recent years. GARG and HAYHOE [11] carried out a full-scale field test at the national airport pavement test facility (NAPTF). The data collected at high loads and low speeds under different temperature conditions revealed that the asphalt layer was subjected to a wide range of dynamic tensile strains from 300 to 2000 ( $10^{-6}$ ), and the ratio of viscous and elastic deformations went up with increasing climatic temperature. AL-QADI *et al.* [9] conducted the full-scale field test at the Virginia Smart Road to measure actual response to loading. The results showed that vehicle speed affected the loading time and horizontal transverse strains measured at the bottom of AC layers. An experimental campaign performed by ISLAM and TAREFDER [12] on an interstate pavement in New Mexico, USA, reported vertical and horizontal strains in the afternoon increased up to 1.88 and 1.41 times, respectively, than those in the morning for the climate condition in New Mexico. GAJEWSKI *et al.* [13] carried out accelerated loading

tests in Poland using Heavy Vehicle Simulator (HVS). The vertical strain in the top of the subgrade and transverse strain at the bottom of asphalt layers were collected under the load of 30–60 kN. According to raw data from 625 000 cycles applied in full-scale instrumented test sections, ELSEIFI *et al.* [14] reported that the repeatability and survivability of stress and strain sensors were acceptable. Furthermore, temperature ejected obvious effect on pavement response.

While the studies are relevant, the mechanisms and applications identified for flexible pavement in other countries cannot be directly applied to evaluate the behavior of asphalt pavements in China due to the distinctions in pavement structure types, climatic conditions, and requirement of pavement structural capacity concerning heavy traffic load. Only a limited number of studies have been specifically conducted to characterize the dynamic properties described by measured responses within full-scale instrumented pavement sections, as detailed next. WANG *et al.* [15] put forward the predicted spatial distribution pattern of the contact stress used as a reference for tire load modeling, which matched the *in situ* pavement conditions. Nevertheless, they did not describe the explicit link between tire load and dynamic strain. DONG and LV [16], took the strain at the bottom of the pavement surface layer as evaluation parameter and conducted *in situ* experiment campaign to explore the dynamic strain response feature of semi-rigid pavement. In another research, 3-D dynamic strain response of asphalt pavement surface based on Fiber Bragg Grating (FBG) technology was studied by DONG *et al.* [17]. Findings of this research quantified the impact of axle load and vehicle speed with relatively same pavement surface type. DONG *et al.* [18] embedded the 3D dynamic strain sensors, which were developed by independent research, into test sections during construction of the experimental road, and then demonstrated the influence of slope location, axle load and speed on the dynamic response of asphalt layers. Generally speaking, these studies considered only the impact of axle load and vehicle speed; besides, the pavement structure included in the above study was relatively analogous.

In order to present the relevant research of this paper, the remaining content is organized as follows. In Sec. 3, the overview of an *in situ* experiment campaign is introduced, including the pavement structures and material compositions of test sections and sensor instrumentation. Section 4 explores the effect of vehicular loading factor and temperature conditions on strain responses. In addition, the impact levels of loading factors were quantified through analysis of variance for orthogonal array tests. Finally, the summary of the results in the range of field tests conducted in this study and corresponding conclusions are presented in Sec. 5.

### 3. TEST SECTIONS AND INSTRUMENTATION

#### 3.1. Test sections

The broad overview of a representative base type for a flexible pavement served as a basis for three typical asphalt pavement structures, namely semi-rigid base (S1), inverted base (S2) and compound base asphalt pavement (S3), which were constructed under the same subgrade conditions with the relatively gentle longitudinal slope. The test road is a two-way highway with four lanes, in which the three types of typical asphalt pavement have been constructed continually. Each pavement structure has a length of 300 m. The detailed pavement structures and the materials used in each layer are shown in Fig. 1.

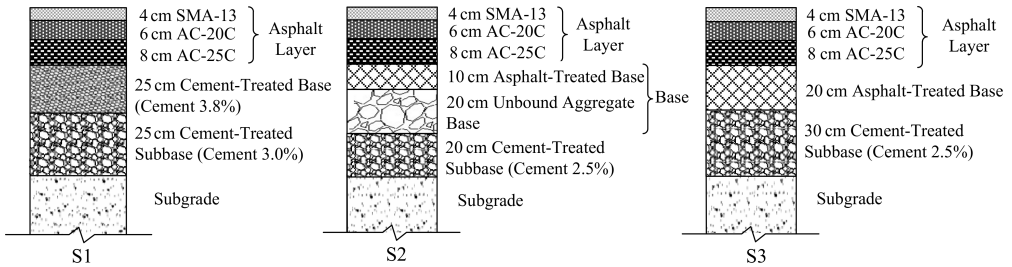


FIG. 1. Pavement structures and materials compositions.

#### 3.2. Sensor installations

A type of dynamic asphalt strain gauges (ASGs), which was produced by Applied Geomechanics Inc. from the USA, was selected as test sensors to capture dynamic horizontal tensile strains, focusing on the accuracy, stability and practicability of raw data. Utilizing four active elements of a Wheatstone bridge circuit, this resistance gauges compensates for temperature, rejects bending strain, and its general specifications are shown in Table 1. The dimensions of ASGs and its real object are shown in Fig. 2.

Table 1. Specifications of ASG.

| Technical indicators   | Values                                   |
|--|--|
| Bridge circuit   | Four active 350 $\Omega$ strain gauges   |
| Range ( $10^{-6}$ )  | $> \pm 2000$                             |
| Sensitivity at 1000, $10^{-6}$ [ $\text{mV} \cdot \text{V}^{-1}$ ] | About 1.3                                |
| Excitation [V]   | Up to 5                                  |
| Temperature range [ $^{\circ}\text{C}$ ]                           | $-34 \sim 200$                           |
| Lead wire  | 24 AWG, twisted four-wire with shielding |

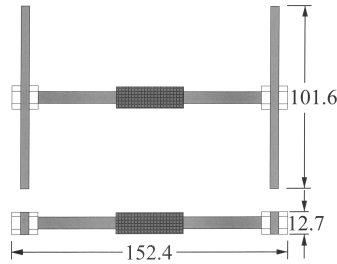


FIG. 2. Dimensions of ASG (unit: mm).

The temperature data within AC layers were monitored using the embedded thermocouples. The infrared thermometer was used to measure temperature on the surface. The pavement temperature condition was quantified as the mean value of the temperature data collected on the surface, within the surface, and at the bottom of the surface layer. To measure horizontal longitudinal and transverse tensile strains, four ASGs were placed at the AC bottom of each pavement structure. The vertical layout of thermocouples and ASGs located in cross-section of pavement is shown in Fig. 3. Figure 4 illustrates the horizontal layout of strain gauge instrumentation. As can be seen, the strain gauges are located in the left wheel path on the middle lane. This was determined based on survey results of the wheel path and the rutting position. During the field testing with vehicular loads, a large number of data on tensile strain pulses were collected utilizing the high-frequency data acquisition system.

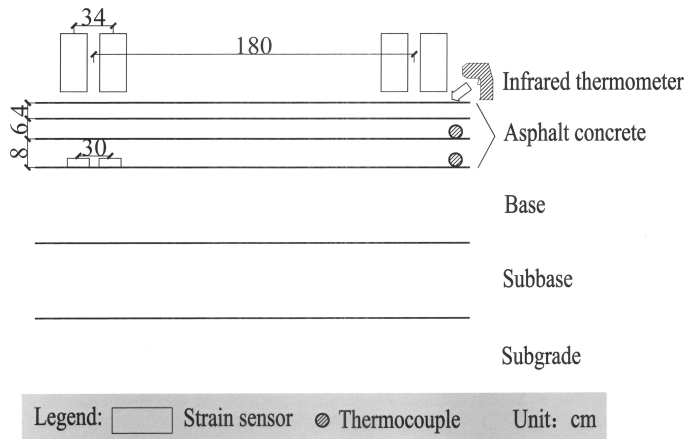


FIG. 3. Vertical layout of embedded sensors.

The reliability of field test was validated using measured strain responses from parallel experiments under vehicular loading with a speed of 60 km/h and an axle load of 100 kN, at a relatively consistent temperature around 15°C.

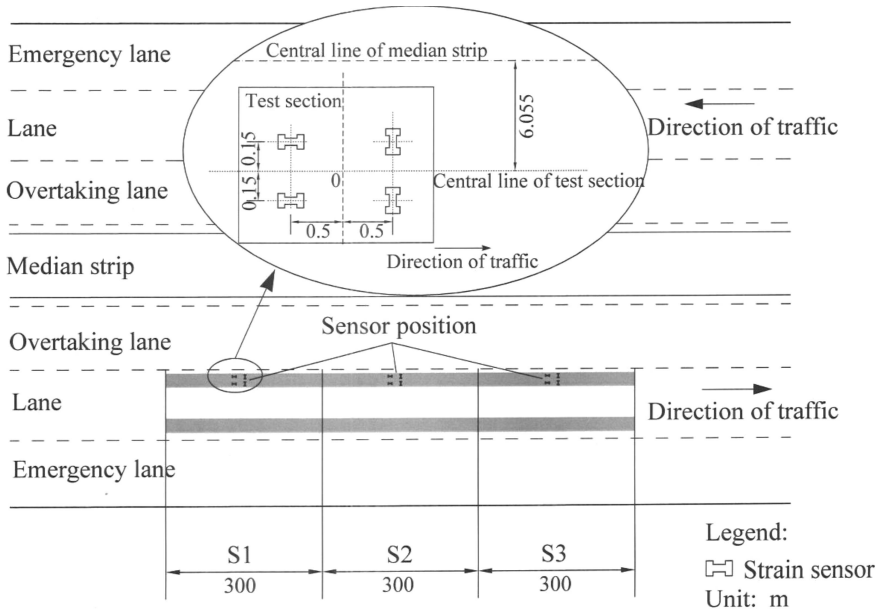


FIG. 4. Horizontal layout of ASGs.

The pavement temperature condition was. The results of the six parallel tests shown in Table 2, which are stable with relatively small standard deviation, manifest excellent repeatability for the field test approach.

**Table 2.** Results from validation tests.

| Test number | Strain ( $\times 10^{-6}$ ) | Data analysis |                    |                          |
|-------------|-----------------------------|---------------|--------------------|--------------------------|
|             |                             | Mean          | Standard deviation | Variable coefficient [%] |
| 1           | 17.1                        | 15.62         | 1.53               | 9.80                     |
| 2           | 13.8                        |               |                    |                          |
| 3           | 14.2                        |               |                    |                          |
| 4           | 14.9                        |               |                    |                          |
| 5           | 17.4                        |               |                    |                          |
| 6           | 16.3                        |               |                    |                          |

It should be noted that field tests are replicated three times for every vehicular loading pass under a specific condition. The maximum value from these three tests was taken as the corresponding measured value to minimize the deviation caused by lateral displacement with respect to the location of the strain gauge when test vehicle passed through instrumented test sections.

## 4. EXPERIMENTAL RESULTS AND DISCUSSIONS

## 4.1. Typical ASGs response

Take S1 as an example, the time-varying strain pulse signals of longitudinal and transverse strain at the bottom of AC surface courses are shown in Fig. 5. The pulse signal captured from each test section was similar. Findings are concluded as follows:

- 1) The acquired strain time history characterizes the dynamic response induced by vehicular loading, which manifests neither horizontal longitudinal nor transverse strain pulses are completely symmetrical with respect to the traffic direction. In terms of the horizontal longitudinal strain, there is one compression zone before the passage of axle load over the ASGs within asphalt layers. However, the magnitude of the compression is small relative to the tension zone. Compared with the longitudinal strain pulse, the measured transverse strain is in tension with no compression zone. Due to the viscoelastic properties of asphalt layers, the strain response presents a delayed recovery process after the load passage and then goes down slowly to the initial value.
- 2) Under the rear tandem axle load, because the small spacing between the two axles leads to the passage of the second axle before the strain induced by the first axle is fully recovered, the strain pulse curve has a bimodal feature.
- 3) The level of measured maximum horizontal tensile longitudinal strain is higher than the transverse strain, which is consistent with the result from the subsequent FWD tests. Part of the reason for this variance between the longitudinal and transverse strains may be attributed to the pavement

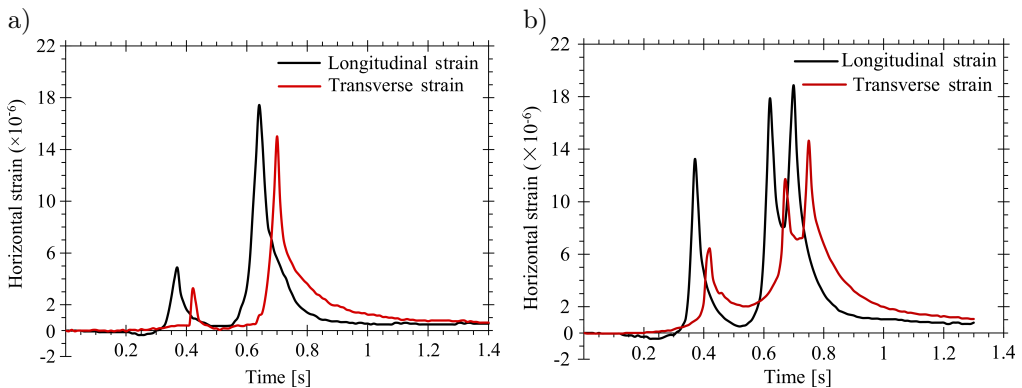


FIG. 5. Typical longitudinal and transverse strain pulse under vehicular loading: a) truck loading with single rear axle, b) truck loading with tandem rear axle.

geometry, as the length of pavement structure is much longer than the width.

During the FWD testing process, the FWD bearing plate was strictly aligned above a specific embedded ASG. Figure 6 illustrates a typical measured strain evolution over time under the Falling Weight Deflectometer (FWD) with six load drops loading sequence (2 drops at 30 kN, 1 drop at 40 kN, 50 kN, 60 kN, and 70 kN, respectively), which was captured in S1 pavement at the temperature of 12°C. The measured strain pulses corresponding to six FWD load drops are similar in shape under different load levels.

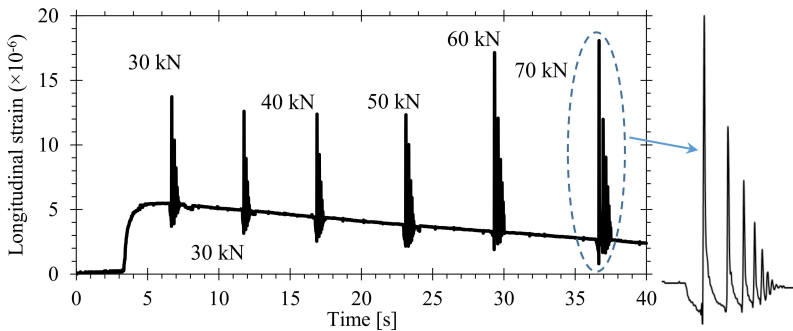


FIG. 6. Typical measured strain response under the increasing FWD load levels.

As detailed in Fig. 6, there is compression at first of the measure strain evolution, then obvious maximum tension and subsequently gradually decreased bounce response. The initial relative compression strain may be attributed to the temporarily released gravity of the heavy hammer before it impacts the bearing plate. The strain reaches the first peak when the hammer hits the bearing plate, then decreases due to the upward rebound of the bearing plate, and then in attenuated oscillation due to vibration of the falling weight. It is similar to the case under vehicular loading that there is an asymmetry on the measured asphalt strain within each pulse cycle in relation to viscoelastic properties of asphalt materials.

#### 4.2. Effects of vehicular loading factors on dynamic strains

In order to investigate the effects of vehicular loading factors on measured strains, a set of field tests were conducted at a relatively consistent temperature (13–15°C).

*4.2.1. Speed and axle load.* Figure 7 presents the effects of vehicular speed and axle load on the maximum measured horizontal transverse strain and the longitudinal one, extracted from strain pulses.

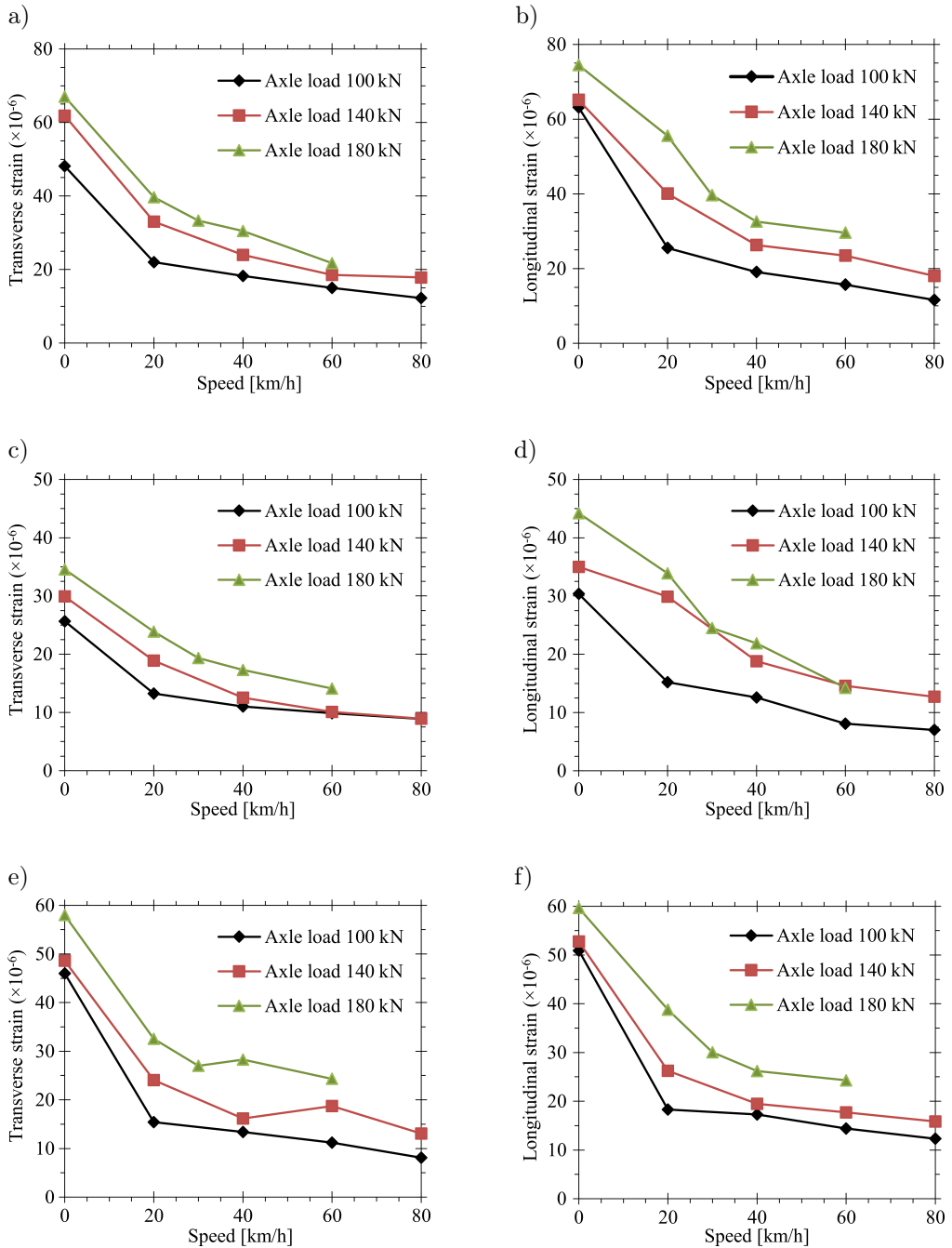


FIG. 7. Variation of strain responses under various axle load and speed levels: a) transverse strains in S1, b) longitudinal strains in S1, c) transverse strains in S2, d) longitudinal strains in S2, e) transverse strains in S3, f) longitudinal strains in S3.

The following observation can be made from Fig. 7a and 7b for S1 pavement:

- 1) The measured tensile strain caused by static loading is obviously higher than the strain under dynamic vehicular loading. Take, for instance, the 100 kN axle load. The maximum transverse tensile strain at the speed of 80 km/h is 25.4% of that under static loading. Moreover, as for the maximum longitudinal strain, the corresponding proportion is only 20%. Thus, the real response to the dynamic loading is so different from the static one that the static loading pattern cannot accurately characterize the actual traffic situation when designing and analyzing pavement structure based on empirical and mechanistic methods.
- 2) The measured strains in the longitudinal and the transverse direction follow a similar trend, along with the change of speed. As the speed increases, the strain response at the bottom of AC layers decreases gradually. It indicates that the material is viscoelastic. Compared to the strain response to static loading or dynamic loading at low speed, the strain response to vehicular loading at high speed develops during a shorter period of time. Therefore, the asphalt layer acts stiffer under vehicular loading at high speed, resulting in smaller strains. For the detailed changes, when the speed increases from zero to 20 km/h, the strain response decreases significantly. However, the downtrend of strain in relation to the increase of speed slows down. Take the axle load of 100 kN as an example, the speed growth from zero to 20 km/h leads to a decrease in the longitudinal strain of approximately 56.5%. After that, as the speed goes up from 20 km/h to 80 km/h with an increment of 20 km/h, the reduction rate of strain response decreases to the range of 21.7–26.9%.
- 3) As the vehicular speed remained, the strain response goes up with growing axle load. Under the strain to static loading, the longitudinal strain and the transverse strain induced by vehicular loading with 180 kN axle load are 1.2 times and 1.4 times of those generated under an axle load of 100 kN, respectively. Conversely, under a dynamic loading at a speed of 20 km/h through 60 km/h, the longitudinal strain under 180 kN axle load increases to 1.7~2.2 times of those under an axle load of 100 kN, and the transverse strain increases to 1.7~1.9 times under the same conditions compared with the longitudinal strain. These results indicate that the influence of the axle load on the tensile strain under dynamic loading conditions is greater than that under static loading conditions, which may be due to the fact that the vehicular loading consists of static axle load and impact load with vibration. Not only can the increase of axle load level raise the tire force, but also enhance the self-stiffness of the tire. Accordingly, there is an enhanced instantaneous effect with vibration as test truck passes over

the position of asphalt gauges, so that the axle load under dynamic mode exerts a more significant influence on the strain response than the static load.

Compared with S1, the measured strains in S2 and S3 follow the same pattern, along with the change of speed and axle load. The following conclusions can be drawn:

- 1) There is a linear relationship between the measured strains and the logarithm of speed, which is described by the regression equation shown as Eq. (4.1)

$$(4.1) \quad \varepsilon = A \ln V + B,$$

where  $\varepsilon$  is strain response,  $V$  is vehicular speed,  $A$  and  $B$  are regression coefficients, respectively.

The regression coefficients  $A$  and  $B$  are shown in Table 3. The reduction rate along with increasing speed in light of the slope of  $\varepsilon - \ln V$  liner equation manifests that the higher the axle load level is, the faster the strain value decreases with the increase of speed.

**Table 3.** Regression coefficients of linear equations.

| Pavement type | Regression coefficients | Longitudinal direction |          |          | Transverse direction |          |          |
|---------------|-------------------------|------------------------|----------|----------|----------------------|----------|----------|
|               |                         | 10t                    | 14t      | 18t      | 10t                  | 14t      | 18t      |
| S1            | $A$                     | -9.7100                | -15.3800 | -23.6500 | -8.5500              | -11.4600 | -16.5200 |
|               | $B$                     | 54.7900                | 85.2700  | 123.1600 | 48.3260              | 66.6600  | 90.2500  |
|               | $R^2$                   | 0.9910                 | 0.9727   | 0.8953   | 0.9617               | 0.9688   | 0.9771   |
| S2            | $A$                     | -6.2600                | -12.6000 | -17.3400 | -3.9200              | -7.7100  | -11.3400 |
|               | $B$                     | 34.5200                | 66.7700  | 85.0900  | 25.0100              | 41.2400  | 58.1000  |
|               | $R^2$                   | 0.9273                 | 0.9741   | 0.9801   | 0.9980               | 0.9879   | 0.9823   |
| S3            | $A$                     | -4.2300                | -7.4470  | -13.2100 | -4.8600              | -6.2900  | -8.4400  |
|               | $B$                     | 31.5800                | 48.0440  | 76.6600  | 30.1700              | 41.6000  | 58.4600  |
|               | $R^2$                   | 0.8823                 | 0.9721   | 0.9051   | 0.9480               | 0.7480   | 0.81222  |

- 2) The longitudinal strain at the bottom of AC layers under vehicular loading is greater than the transverse one, which is in an agreement with the results from TIMM and PRIEST [19]. It indicates that longitudinal tensile strains resulting in transverse cracking are more responsible for fatigue cracking than transverse strains. The correlations of the measured longitudinal strain  $\varepsilon_L$  with the transverse strain  $\varepsilon_T$  for the three types of pavements fitted by linear regression equations are shown in Table 4.

**Table 4.** Correlation equations of longitudinal strains with transverse strains.

| Pavement type | Linear fitting equation                       | $R^2$ |
|---------------|---|-------|
| S1            | $\varepsilon_L = 1.103\varepsilon_T + 1.1845$ | 0.972 |
| S2            | $\varepsilon_L = 1.251\varepsilon_T - 0.767$  | 0.906 |
| S3            | $\varepsilon_L = 1.008\varepsilon_T + 2.653$  | 0.972 |

*4.2.2. Significance analysis of influential factors over strain response.* To assess the impact level of speed, axle load, tire inflation pressure, and their interactions on tensile strains in a feasible way, an orthogonal experimental design was carried out to reduce the number of field tests. In this design, the three factors, each with two levels, are selected for each pavement structure, as shown in Table 5. The pavement temperature is considered as a constant variable during the testing process.

**Table 5.** Factors and levels of orthogonal test.

| Level | Speed [km/h] | Axle load [kN] | Tire inflation pressure [kPa] |
|-------|--------------|----------------|-------------------------------|
| 1     | 20           | 100            | 700                           |
| 2     | 60           | 180            | 1300                          |

As shown in Table 6, a table template from Taguchi Orthogonal Arrays [20] with seven columns (factors) and eight rows (test number) was used, in which each factor such as speed (A), axle load (B), tire inflation pressure (C), and their interaction ( $A \times B$ ,  $A \times C$  and  $B \times C$ ) was assigned to a column, eight loading factor combinations being available. Besides that, a blank column of 7 was set to conduct error analysis. Note that since the longitudinal strain is greater than the

**Table 6.** Test program and results of test.

| Test No. | Factors |   |              |   |              |              |   | Strain ( $\times 10^{-6}$ ) |      |      |
|----------|---------|---|--------------|---|--------------|--------------|---|-----------------------------|------|------|
|          | A       | B | $A \times B$ | C | $A \times C$ | $B \times C$ |   | S1                          | S2   | S3   |
|          | 1       | 2 | 3            | 4 | 5            | 6            | 7 | 8                           | 9    | 10   |
| 1        | 1       | 1 | 1            | 1 | 1            | 1            | 1 | 25.50                       | 15.2 | 18.3 |
| 2        | 1       | 1 | 1            | 2 | 2            | 2            | 2 | 26.10                       | 16.1 | 17.9 |
| 3        | 1       | 2 | 2            | 1 | 1            | 2            | 2 | 55.50                       | 33.9 | 38.8 |
| 4        | 1       | 2 | 2            | 2 | 2            | 1            | 1 | 65.30                       | 36.5 | 40.2 |
| 5        | 2       | 1 | 2            | 1 | 2            | 1            | 2 | 15.75                       | 8.1  | 14.4 |
| 6        | 2       | 1 | 2            | 2 | 1            | 2            | 1 | 16.70                       | 8.5  | 16.2 |
| 7        | 2       | 2 | 1            | 1 | 2            | 2            | 1 | 32.59                       | 21.9 | 26.2 |
| 8        | 2       | 2 | 1            | 2 | 1            | 1            | 2 | 39.40                       | 25.4 | 30.8 |

transverse one, only the longitudinal strain is studied in the subsequent analysis of the dynamic strain at the bottom of asphalt layers.

To investigate which loading factors or their interaction significantly affect the strain response at the bottom of asphalt layers, analysis of variance (ANOVA) for orthogonal array tests was performed through a general procedure following these basic steps:

- 1) The total sum of squared deviations  $SS_T$  is decomposed into two sources: one is the sum of squared deviations  $SS_j$  concerning each factor calculated as Eq. (4.2) and another one is the sum of squared error  $SS_e$ , which is the blank column's sum of squared deviations in Table 6

$$(4.2) \quad SS_j = \frac{\sum_{i=1}^t K_{ij}^2}{n} - \frac{S^2}{N},$$

where  $K_{ij}$  is the sum of strain response for factor  $j$  at level  $i$ ,  $n$  is the number of factor  $j$  data at level  $i$ ,  $t$  is the number of levels,  $S$  is the sum of all data and  $N$  is the number of all data.

- 2) The mean of squared deviations  $\overline{SS_j}$  due to aforementioned factors and mean square error  $\overline{SS_e}$  can be calculated through Eq (4.3), respectively

$$(4.3) \quad \overline{SS_j} = \frac{SS_j}{f_j}, \quad \overline{SS_e} = \frac{SS_e}{f_e},$$

where  $f_j$  is the number of degrees of freedom associated with factor  $j$ ,  $f_j = t - 1$ , and  $f_e$  is the number of degrees of freedom concerning errors.

- 3) The  $F$  value referred to as  $F_j$  for each factor is the ratio of  $\overline{SS_j}$  and  $\overline{SS_e}$  as shown in Eq. (4.4), which can quantify the significance level for different factors and their interaction based on the designated significance levels of 0.01 and 0.05

$$(4.4) \quad F_j = \frac{\overline{SS_j}}{\overline{SS_e}}.$$

The results of ANOVA for S1, S2 and S3 are shown in Table 7.

According to the results of the ANOVA for strain response, it can be found that in the range of loading factors included in this study, the effect of axle load seems to be dominant for each asphalt pavement type. For S1, the changes of axle load, speed and their interaction referred to as A, B and  $A \times B$  have highly significant effects on measured strain response, on which the changes of tire inflation pressure (C) and the interaction of axle load and tire pressure ( $B \times C$ ) have normally significant effects. However, the interaction of speed and tire pressure

Table 7. Results of the ANOVA for strain responses.

| Pavement type | Symbol                              | Degrees of freedom | Sum of squares           | Contribution [%] | Mean square | F value | F critical value |        | Significance level |
|---------------|-------------------------------------|--------------------|--------------------------|------------------|-------------|---------|------------------|--------|--------------------|
|               |                                     |                    |                          |                  |             |         | 0.05             | 0.01   |                    |
| S1            | A                                   | 1                  | 578.2                    | 25.8             | 578.2       | 525.6   |                  |        | **                 |
|               | B                                   | 1                  | 1481.0                   | 66.1             | 1481.0      | 1346.4  |                  |        | **                 |
|               | A × B                               | 1                  | 109.9                    | 4.9              | 109.9       | 99.9    | 18.5             | 98.5   | **                 |
|               | C                                   | 1                  | 40.7                     | 1.8              | 40.7        | 37.0    |                  |        | *                  |
|               | B × C                               | 1                  | 28.5                     | 1.3              | 28.5        | 25.9    |                  |        | *                  |
|               | A × C } Error <sup>Δ</sup><br>Error | 1 } 2<br>1 } 1     | 0.9 } 2.2<br>1.3 } 1.3   | 0.1              | 1.1         |         |                  |        |                    |
| S2            | A                                   | 1                  | 178.6                    | 22.1             | 178.6       | 893.0   |                  |        | **                 |
|               | B                                   | 1                  | 609.0                    | 75.5             | 609.0       | 3045.0  |                  |        | **                 |
|               | A × B                               | 1                  | 8.8                      | 1.1              | 8.8         | 44.1    | 18.5             | 98.5   | *                  |
|               | C                                   | 1                  | 6.9                      | 0.8              | 6.9         | 34.2    |                  |        | *                  |
|               | B × C                               | 1                  | 2.9                      | 0.4              | 2.9         | 14.4    |                  |        | —                  |
|               | A × C } Error <sup>Δ</sup><br>Error | 1 } 2<br>1 } 1     | 0.02 } 0.3<br>0.25 } 0.3 | 0.1              | 0.2         |         |                  |        |                    |
| S3            | A                                   | 1                  | 95.2                     | 12.9             | 95.2        | 761.8   |                  |        | *                  |
|               | B                                   | 1                  | 598.6                    | 80.8             | 598.6       | 4788.6  |                  |        | **                 |
|               | A × B                               | 1                  | 33.6                     | 4.5              | 33.6        | 269.0   | 161.4            | 4052.0 | *                  |
|               | C                                   | 1                  | 6.8                      | 0.9              | 6.8         | 54.8    |                  |        | —                  |
|               | A × C                               | 1                  | 3.6                      | 0.5              | 3.6         | 29.2    |                  |        | —                  |
|               | B × C                               | 1                  | 2.6                      | 0.4              | 2.6         | 21.2    |                  |        | —                  |
| Error         | 1                                   | 0.1                | 0.1                      | 0.1              | 0.1         |         |                  |        |                    |

Note: As for significance level,  $F_j > F_{0.01}$  denotes the effect of this factor is highly significant, represented by “\*\*”;  $F_{0.05} < F_j < F_{0.01}$  denotes its influence is significant, represented by “\*”;  $F_j < F_{0.05}$  denotes its influence is not significant, represented by “—”.

(B × C) had no significant effect on strain responses. Accordingly, the factors with highly significant effects for S2 are A and B. In terms of S3, only the factor B has highly significant effects on measure strain response. S1 and S2 pavements follow a similar rule that the impact level of each factor and their interaction on the strain response is ordered as follow: B > A > A × B > C > B × C > A × C. As for S3, the corresponding order is B > A > A × B > C > A × C > B × C.

#### 4.3. Effects of pavement temperature on the measured strain

The strain responses to a constant vehicular loading process with a speed of 60 km/h, a single axle load of 100 kN, and a tire inflation pressure of 700 kPa under various temperature conditions are presented in Fig. 8.

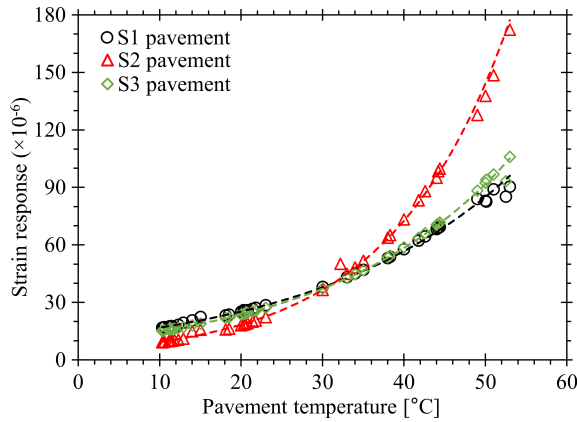


FIG. 8. Temperature dependency of strain responses.

The strain is found to increase exponentially with an increase in temperature so that the pavement temperature (independent variable) and the strain response (dependent variable) could be well fitted to the exponential model shown in Eq. (4.5)

$$(4.5) \quad \varepsilon = e^{a \cdot T + b},$$

where  $\varepsilon$  is the longitudinal strain at the bottom of asphalt layers,  $10^{-6}$ ;  $T$  is the pavement temperature, °C;  $a$  and  $b$  are regression coefficients.

The conversion of strain responses from actual temperature level to the reference temperature conditions can be defined as conversion factor  $K_T$  through Eq. (4.6)

$$(4.6) \quad K_T = \frac{\varepsilon_r}{\varepsilon_m} = e^{a \cdot (T_r - T_m)},$$

where  $\varepsilon_r$  is the longitudinal strain at the reference temperature referred to as  $T_r$ ,  $10^{-6}$ ;  $\varepsilon_m$  is the longitudinal strain at the measured field temperature referred to as  $T_m$ ,  $10^{-6}$ .

According to Eq. (4.6), the regression coefficient  $a$  shown in Table 8 were determined at the reference temperature of  $20^\circ\text{C}$ . The temperature dependency of the strain response can be quantified through the temperature conversion factor  $K_T$ .

**Table 8.** Regression results of the temperature conversion factors.

| Pavement type | Regression coefficient |        | Conversion factor $K_{20}$    |
|---------------|------------------------|--------|-------------------------------|
|               | $a$                    | $R^2$  |                               |
| S1            | 0.03921                | 0.9948 | $e^{0.0392 \cdot (20 - T_m)}$ |
| S2            | 0.06628                | 0.9883 | $e^{0.0662 \cdot (20 - T_m)}$ |
| S3            | 0.04465                | 0.9877 | $e^{0.0447 \cdot (20 - T_m)}$ |

Note: According to Eq. (4.6), the conversion factor  $K_{20}$  were determined at the reference temperature of  $20^\circ\text{C}$ .

To be more specific, the greater the regression coefficient  $a$  pertaining to each pavement structure is, the more sensitive to temperature variation the strain response at the AC bottom is. In other words, the higher value of the regression coefficient  $a$  represents a worse adaptivity to temperature variation. The temperature dependency levels of the aforementioned three types of pavement structures are arranged in descending order as S2, S3 and S1. The semi-rigid base pavement (S1), presenting the best temperature adaptability in strain responses, is of paramount importance for the pavement service life based on the bottom-up fatigue cracking in the high-temperature region or in areas with extreme seasonal variation in temperature.

All in all, the conversion factor  $K_T$  determined above can be used to make the conversion of measured strains between the response under a non-standard temperature condition and the one at a reference temperature.

## 5. CONCLUSION

The following conclusions can be drawn from the analysis as mentioned above:

- 1) An asphalt concrete layer under the vehicular or the FWD loading is subjected to horizontal tensile strains, presenting an asymmetry in strain evolution over time. Besides, the longitudinal strain at the bottom of asphalt layers generated by the vehicular loading is greater than the strain response in the transverse direction, implying that a transverse fatigue cracking would occur from the bottom of asphalt layers resulting from the greater generated strain in the longitudinal direction.

- 2) As temperature conditions remain constant, the measured strain response for each pavement structure goes up with increasing axle load and decreases with growing speed. The measured strain responses present a linear correlation with the natural logarithm of speed, which manifests the higher the axle load level is, the faster the strain value decreases with the increase of speed.
- 3) Using analysis of variance (ANOVA) for orthogonal array tests, the impact levels of loading factors on strain responses for S1 (semi-rigid base pavement) and S2 (inverted base pavement) follow a similar order: B (axle load) > A (speed) > A × B (speed and axle load) > C (tire inflation pressure) > B × C (axle load and tire inflation pressure) > A × C (speed and tire inflation pressure). As for S3 (compound base pavement), the corresponding order is B > A > A × B > C > A × C > B × C.
- 4) The measured strain increases exponentially with the growing temperature. In light of the definition of the temperature conversion factor, which contributes to quantifying the sensitivity of the temperature dependency of strain responses, the temperature dependency levels of pavement structures included in this study are ranked as S2 > S3 > S1.

#### ACKNOWLEDGEMENTS

This work was supported by the National Natural Science Foundation of China (No. 51378438) and the scientific research funding from Education Department of Sichuan Province (No. 16ZB0513). The author also wishes to thank the China Scholarship Council ([2017]5086, and No. 201708515023) for financial support to visit the University of South Florida, USA.

#### REFERENCES

1. MONISMITH C.L., *International conferences-twenty five years of contributions to asphalt concrete pavement design and rehabilitation*, Proceedings of 6th International Conference on Structural Design of Asphalt Pavements, **2**: 2-18, 1987.
2. YAO Z.K., *Structural design of asphalt pavements* [in Chinese], China Communications Press, Beijing, 2011.
3. ARA (Applied Research Associates), *Guide for mechanistic-empirical design of new and rehabilitated pavement structures*, NCHRP 1-37A Final Rep., Transportation Research Board, Washington, DC, 2004.
4. NIKI D.B., STEPHANOS V.T., GEORGE D.H., *Fatigue cracking failure criterion for flexible pavements under moving vehicles*, Soil Dynamics and Earthquake Engineering, **90**: 476-479, 2016.

5. FUNDOWICZ P., MICHER J., *Semi-empirical Model of tire-pavement contact*, Engineering Transactions, **48**(3): 205–220, 2000.
6. WOREL B.J., CLYNE T.R., *Low-volume road performance related to traffic loadings at Minnesota road research project*, Transportation Research Record, **1989**(2): 300–305, 2007.
7. PRIEST A.L., TIMM D.H., *A full-scale pavement structural study for mechanistic-empirical pavement design*, Journal of the Association of Asphalt Paving Technologists, **74**: 519–556, 2005.
8. WILLIS J.R., TIMM D.H., *Development of stochastic perpetual pavement design criteria*, Journal of the Association of Asphalt Paving Technologists, **79**(1): 561–595, 2010.
9. AL-QADI I.L., LOULIZI A., ELSEIFI M., LAHOUAR S., *The Virginia SMART ROAD: the impact of pavement instrumentation on understanding pavement performance*, Journal of the Association of Asphalt Paving Technologists, **73**(3): 427–465, 2004.
10. SARGAND S., GREEN R., KHOURY I., *Instrumenting Ohio test pavement*, Transportation Research Record: Journal of the Transportation Research Board, **1596**: 23–30, 1997.
11. GARG, N., HAYHOE G.F., *Asphalt concrete strain responses at high loads and low speeds at the national airport pavement test facility (NAPTF)*, Proceedings of the 2001 ASCE Airfield Pavement Specialty Conference, 2001.
12. ISLAM, M.R., TAREFDER R.A., *Measuring thermal effect in the structural response of flexible pavement based on field instrumentation*, International Journal of Pavement Research and Technology, **6**(4): 274–279, 2013.
13. GAJEWSKI M., BAŃKOWSKI W., SYBILSKI D., *Analysis of Fatigue Damage on Test Sections Submitted to HVS Loading*, The Baltic Journal of Road and Bridge Engineering, **8**(4): 255–262, 2013, doi: 10.3846/bjrbe.2013.33.
14. ELSEIFI M.A., MOHAMMAD L.N., ZHANG Z., *Assessment of Stress and Strain Instrumentation in Accelerated-Pavement Testing*, International Journal of Pavement Research and Technology, **5**(2): 121–127, 2012.
15. WANG Y., SUN T., LU Y., SI C., *Prediction for Tire-Pavement Contact Stress under Steady-State Conditions based on 3D Finite Element Method*, Journal of Engineering Science and Technology Review, **9**(4): 17–25, 2016.
16. DONG Z.H., LV P.M., *Influence of axis's load and speed on dynamic response of semi-rigid base of asphalt pavement* [in Chinese], Journal of Chang'an University (Natural Science Edition), **28**(1): 32–36, 2008.
17. DONG, Z.J., LIU H., TANG Y.Q., *Field Measurement of Three-Direction Strain Response of Asphalt Pavement* [in Chinese], Journal of South China University of Technology (Natural Science Edition), **37**(7): 46–51, 2009.
18. DONG Z.H., LV P.M., LIU X., *Test on dynamic response of asphalt pavement at large longitudinal slope section* [in Chinese], Journal of Chang'an University (Natural Science Edition), **33**(4): 7–11, 2013.

19. TIMM H.P., PRIEST A.L., *Flexible Pavement Fatigue Cracking and Measured Strain Response at the NCAT Test Track* [in Chinese], in Proceedings of the 87th TRB Annual Meeting, 2008.
20. QIU Y.B., *Experimental design and data processing* [in Chinese], Science and Technology of China Press, Beijing, 2008.

*Received October 17, 2018; accepted version December 12, 2018.*

---

*Published on Creative Common licence CC BY-SA 4.0*

